Physical Education, Health and Social Sciences

https://journal-of-social-education.org E-ISSN: 2958-5996

P-ISSN: 2958-5988

Local Meshless Method For Elliptic Interface PDEs Via RBFs Augmented with Pascal Polynomials

Mujahid Khan[1]

[1] Department of Basic Sciences, University of Engineering and Technology, Peshawar, Pakistan.

DOI: https://doi.org/10.63163/jpehss.v3i4.797

Abstract

The solution of elliptic partial differential equations (PDEs) with sharp interfaces presents significant challenges, especially when the domain is irregular or complex, as gradients may not be well-defined at corners and may exhibit discontinuous derivatives. The local meshless method is a promising approach for addressing such difficulties. In [1], a Radial Basis Function collocation technique was proposed for the solution of 2nd-order elliptic interface PDEs having sharp corners, using stencils at the interface designed to handle corner discontinuities. While this method demonstrated notable improvements over conventional approaches, there are instances where accuracy falls short of expectations. In this work, we enhance the local RBF method by incorporating Pascal polynomials, aiming to improve numerical solutions for elliptic interface PDEs. We evaluate the method's effectiveness in handling complex geometries and its adaptability to various interface shapes.

Keywords: Radial Basis Functions (RBFs), Local Meshless Method, Pascal Polynomials

1. Introduction

To solve PDEs numerically like Poisson-Boltzmann equation having non-smooth interfaces is crucial due to its applications in modeling various physical phenomena. These models often involve geometric singularities such as surfaces of self-intersecting and cusps, which can lead to accuracy challenges. In regions near these geometric singularities, the electric field becomes singular, notably at sharp corners of 2D conductors and the tips of electrodes [2]. Solving such elliptic PDEs with non-smooth interfaces and discontinuous coefficients is complex but vital for many applications, including engineering [3], waveguide analysis [4], friction modeling and electromagnetic wave propagation and scattering [5, 6]. This research paper introduces a novel work that combines Radial Basis Functions with high order polynomials to reduce errors.

In this research, we focus on a 2-D elliptic PDEs on planar domains having sharp interfaces.

The PDEs which are considered are,

$$\nabla.(\beta_1 \nabla v_1) + k_1 v_1 = f_1, \text{ in } \Omega_1, \quad ...(1)$$
$$\nabla.(\beta_2 \nabla v_2) + k_2 v_2 = f_2, \text{ in } \Omega_2,$$
$$v_2 = h, \text{ on } \partial\Omega,$$
$$-(v_1 - v_2) = g_1, \text{ on } \Gamma,$$
$$-(\beta_1 \nabla v_1.n_1 - \beta_2 \nabla v_2.n_2) = g_2, \text{ on } \Gamma.$$

In the above problem v_1, v_2, g_1 and g_2 being functions of x and y, n_1 and n_2 indicate the outward normals to the domain. Here, $\Omega = \Omega_1 \cup \Omega_2$ and $\mathbf{\Gamma} = \Omega_1 \cap \Omega_2$.

Such elliptic PDEs are extensively used to model various real-world phenomena, including image processing [7], population dynamics [8], and applications in science and engineering [3]. They also play a crucial role in waveguide analysis [4], electromagnetic wave propagation and scattering, as well as friction modeling [5, 6].

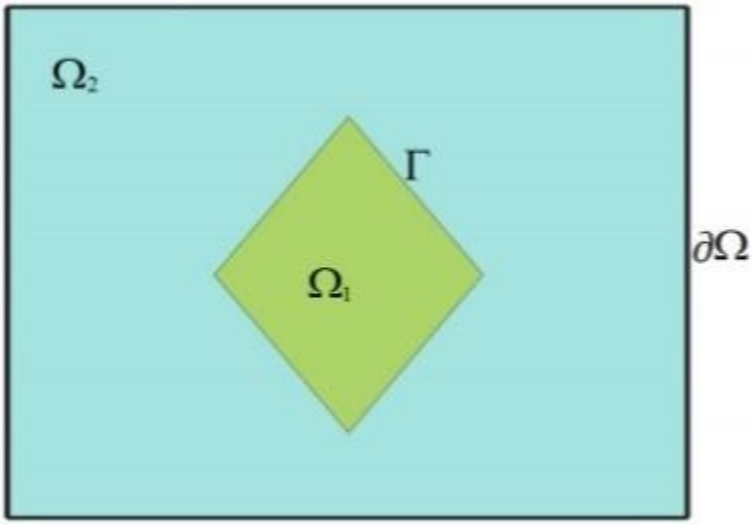

Figure 1: The Computational domain in which the given problem should be taken.

The conventional numerical methods designed for the solutions perform poorly in case of inter- face problems. Solving elliptic interface PDEs presents ongoing challenges, highlighting the need for simpler and more efficient techniques. A critical requirement is the development of methods that produce symmetrically positive definite systems of equations, facilitating the solution of these complex interface issues. Over time, it remains the desire of researchers and mathematicians to develop stable, accurate and convergent methods. the conventional numerical approaches for the numerical solution of PDEs like FDM, FEM and FVM have been developed for the numerical solutions for certain PDEs. In [9], parabolic and elliptic PDEs related to diffusion are tackled, considering interface-embedded domains.

At sharp interface corners, where derivatives do not exist, conventional methods often fail to produce satisfactory results, as noted in [3]. Many finite element methods require mesh refinement near sharp corners, leading to significant memory costs [10]. Additionally, conventional local mesh refinement methods can yield poor results in situations where solutions exhibit high oscillations, such as in electromagnetic wave propagation and scattering, shock wave interactions, and vibration analysis of engineering structures [11]. Developing convergent and accurate inter- face schemes for arbitrary geometries remains a challenging task [2]. For example, a specific finite element formulation for elliptic PDEs with sharp interface edges achieved approximately 0.8th order convergence but struggled with poorly fitted geometries [12].

These challenges have driven us to address the drawbacks and explore methods to control errors and improve convergence. Recently, localized meshless methods have gained attention due to their advantages in numerical solutions for PDEs and certain integral equations. In localized meshless

methods, stencil sizes are adjusted to control errors locally and approximate solutions on overlapping subdomains. A key advantage of meshless methods is their ability to handle irregular geometries and scattered data. Radial Basis Functions (RBFs) are used both locally and globally to approximate solutions. Compared to global meshless methods, localized RBF methods offer computational benefits such as reduced sensitivity to shape parameter choices and efficient banded/sparse matrix representations. Additionally, localized methods provide flexibility in choosing nodal points and stencil sizes to control errors. Nodal points help support the do- main and achieve physical solutions in PDEs that are dominated by some convection effects [13]. Local RBF methods exhibit lower sensitivity to shape parameter selection compared to global methods, indicating that extra caution is needed when using global RBFs for PDE approximations. Achieving both high accuracy and well-conditioned matrices with RBF approximation is challenging [14]. Researchers have developed various algorithms to find optimal shape parameter values [15] or stable methods to reduce sensitivity to shape parameter choices [16], often resulting in reduced computational costs.

In this study, we introduce a robust local differential quadrature meshless approach that demonstrates improved stability characteristics. The domain is partitioned into two interfacial regions, with numerical solutions computed separately in each subdomain. Our method enhances Radial Basis Functions (RBFs) by incorporating Pascal polynomials in case of scattered and uniform nodes. The evaluation of the effectiveness of this meshless method is taken with various RBFs on complex problems having singularities, oscillatory behavior, and sharp corners of the inter- faces. The method is finally compared with other methods from literature and some useful and reasonable results achieved.

2. Numerical Analysis

In this section, RBFs and Pascal polynomials are used for approximation.

2.1 Radial Basis Functions (RBF)

RBFs are mathematical functions, depend upon the distance from a central point, commonly used for interpolation or approximation in numerical analysis and meshless methods.

Radial Basis Functions (RBFs) come in various types with distinct interpolating properties. The choice of RBFs for approximating PDEs depends on specific norms and shape parameters. In this research, we employ two types of RBFs [15] for PDE approximation, including MQ given as below

$$\psi(r) = \quad 1 + (\epsilon r)^2.$$

The Multiquadric RBF is commonly used in meshless methods and interpolation due to its ability to capture both local and global features in the data. The second RBF used in this research is the polyharmonic spline, a family of Radial Basis Functions (RBFs) widely applied in interpolation and meshless methods. The polyharmonic spline RBF is defined as

$$\psi(r) = r^{2\epsilon+1}$$

As discussed above in the RBFs, ϵ represents shape parameter. Also, the nodal distance is taken as $r = ||x - x_j||$, x_j is a point in the computational domain.

2.2 The Local Meshless Technique

To solve elliptic interface PDEs numerically, many conventional methods may struggle to perform optimally. However, the Radial Basis Function-Finite Difference (RBF-FD) method emerges as a leading approach for tackling these problems. In this method the points say $x_i = (x_i, y_i)$ for

i = 1, 2, . . . , N , are further divided as,

$$\Lambda_1 = \{x_i \in \partial\Omega\},$$
$$\Lambda_2 = \{x_i \in \Omega_1\},$$
$$\Lambda_3 = \{x_i \in \Gamma\}, \qquad (2)$$
$$\Lambda_4 = \{x_i \in \Omega_2\}.$$

also N_m for m = 1, 2, 3, 4, shows point following the specific order of Λ_m, subject to the condition that $N_1 + N_2 + N_3 + N_4 = N$. Moreover, it is taken that every subset contains at least one point. In this meshless technique, the nodes are sorted in ascending order based on their distance from a chosen center, after which a set of the closest points is selected for each predefined center $\mathbf{x}_j$, here $j = 1, 2, \ldots, N$, taking Euclidean norm.

We take $x_{k,}$, for $k' = 1,2, \ldots, n$, at the vicinity of stencil around x_j having size n. also we let $(\alpha_1, \alpha_2) = \alpha$ and consider

$$v_i^{\alpha} = \frac{\partial v_i^{(\alpha_1+\alpha_2)}}{\partial x^{\alpha_1} \partial y^{\alpha_2}}.$$

$$\text{Then } \sum_{k'=1}^{n} \left(\lambda_{jk'}^{(\alpha)}\right) v_i(x_k') + \sum_{i,j=1}^{n,i} p_{ij} x^{i-j} y^{j-1} \approx v_i^{\alpha}(x_j), \ldots(3)$$

with some constraints as,

$$\sum_{k'=1}^{n} \lambda_{K'} = \sum_{k'=1}^{n} \lambda_{K'}\, x_{k'} = \sum_{k'=1}^{n} \lambda_{K'}\, y_{k'} = \sum_{k'=1}^{n} \lambda_{K'}\, x_{k'}^2 = \sum_{k'=1}^{n} \lambda_{K'}\, x_{k'} y_{k'=,\ldots,=} \sum_{k'=1}^{n} \lambda_{K'}\, x_{k'}^{k-m} y_{k'}^{m-1} = 0.$$

For the determination of coefficients $\lambda_{jk'}^{(\alpha)}$, we proceed as follows.

Let us take the approximate value in (3) is exact at x_j incase of any RBFs. This consideration leads as follows:

$$\sum_{k'=1}^{n} \left(\lambda_{jk'}^{(\alpha)}\right) \psi_i(x_k') + \sum_{i=1}^{n} 1 \sum_{j=1}^{i} p_{ij} x^{i-j} y^{j-1} = v_i^{\alpha}(x_j), \ i' = 1,2, \ldots, n, \quad \ldots(4)$$

$$\sum_{k'=1}^{n} \lambda_{K'} = \sum_{k'=1}^{n} \lambda_{K'}\, x_{k'} = \sum_{k'=1}^{n} \lambda_{K'}\, y_{k'} = \sum_{k'=1}^{n} \lambda_{K'}\, x_{k'}^2 = \sum_{k'=1}^{n} \lambda_{K'}\, x_{k'} y_{k'=,\ldots,=} \sum_{k'=1}^{n} \lambda_{K'}\, x_{k'}^{k-m} y_{k'}^{m-1} = 0, \ \ldots (5)$$

where $\psi\left(\left|\left|x - x_j\right|\right|\right) = \psi_j(x_i)$ which can be expressed in term of linear combination as having the weight of the stencil as, $\psi_j^{\alpha} = A_j \lambda_j^{\alpha}$, …(6)

in which, $A_j = \begin{matrix} A1_j & B_j \\ B_j^T & 0 \end{matrix}$.

The structure of elements of $\boldsymbol{A}1j$ *is taken as* $\psi_{i'}(x_{k'}) = a_{i'} x_{k'}$, *where* $i', k' = 1,2, \ldots, n$, *and* $\sum_{i,j=1}^{n,i} p_{ij} x^{i-j}\, y^{j-1} = B_j^T$, *in which* $\left(\lambda_{j1}^{\alpha}, \ldots, \lambda_{jn}^{\alpha}, p_{j1}, \ldots, p_{jn}\right)^T = \boldsymbol{\lambda_j^{\alpha}}$, and $\underline{(\psi_1^{\alpha}, \ldots, \psi_n^{\alpha}, 0, \ldots, 0)^T = \boldsymbol{\psi_j^{\alpha}}.}$

The resulting linear system of equations described above must be evaluated for each value of the derivative operator and each nodal point. assume that the matrices Aj having no singularities and finally the weights will be represented as

$$\boldsymbol{A_j^{-1} \psi_j^{\alpha} = \lambda_j^{\alpha}}. \ \ldots(7)$$

This will be utilized to construct weights that fully represent the complete PDE operator defined above is

$$\underline{\beta_l \left(\boldsymbol{\lambda_j^{(2.0)}} + \lambda_j^{(0,2)}\right) + \beta_l^{(1,0)} - k_1 e_1 = \lambda_j^{L}, \text{ L=1,2. } \ldots(8)}$$

Where e_1 is the identity matrix. Similarly,

$$\beta_l\left(\boldsymbol{\lambda_j^{(1.0)}} n_x + \lambda_j^{(0,1)} n_y\right) = \lambda_j^L, \mathrm{L} = 1,2. \quad \ldots(9)$$

The notation (n_x, n_y)represent unit normals in (9). Once the global matrix is constructed, an equation is formulated for each node x_j. The local stencil weights for each node are computed. These weights are then then put off into the desired PDE operator. The local indices denoted by $k = 0,1, \ldots, n$ can be converted to align with their corresponding positions in the global unknowns' vector. The weight pattern is then placed in the appropriate position in the matrix. Let us take B_{qr} in the PDE operator formulated as (1) and their weights from (8) with each rows aligned to$x_j \in \Lambda_q$, in the same way, the columns represent the function weights for values at $x_k \in \Lambda_r$. Similarly, the partition of matrix C_{qr} associated with the interface operator, whose weights are derived from (9). Consider that I_k represents the identity matrix of dimension k and let us take the blocks of zeros sit up to the required sizes, then the overall equation framework become as,

$$\begin{matrix} I_{N_1} & 0 & 0 & 0 & 0 \\ B_{21} & B_{22} & B_{23} & 0 & 0 \\ 0 & 0 & I_{N_3} & -I_{N_3} & 0 \\ 0 & C_{32} & C_{33} & -C_{33} & -C_{34} \\ 0 & 0 & 0 & B_{43} & B_{44} \end{matrix} \begin{matrix} v_1(\Lambda_1) \\ v_1(\Lambda_2) \\ v_1(\Lambda_3) \\ v_2(\Lambda_3) \\ v_2(\Lambda_4) \end{matrix} = \begin{matrix} h(\Lambda_1) \\ f_1(\Lambda_2) \\ g_1(\Lambda_3) \\ g_2(\Lambda_3) \\ f_2(\Lambda_4) \end{matrix} . \quad \ldots(10)$$

Eq (10) is the global matrix, which is asymmetric, sparse, with every equation row containing n elements which are non-zero corresponding to interior nodes and rows correspond to interface conditions of derivative contain $2n$ elements which are non-zero. This system of equation can be solved by a desired method.

3. Numerical Results

In this portion, the proposed methodology is employed to solve selected benchmark 2-D elliptic interface PDEs, to show their efficiency, accuracy and rate of convergence. In the current section we used some symbols like 'ϵ' represents shape parameter, if Multi Quadric (MQ) Radial Basis Function (RBF) is used and it represents power of spline, if Polyharmonic spline is used. Also κ for oscillation in the problem, Grad for gradient, h represents the nodal distance incase of scattered nodes. Also LMM7PP stands for Local Meshless Method using Pascal polynomials of 7th order and LMM9PP stands for Local Meshless Method using Pascal polynomials of 9th order. We added RBF with Pascal polynomial to solve the PDEs numerically. The nodes that are considered are scattered and uniform. For uniform nodes, we take the nodal distance as h which is specified as $\frac{b-a}{N}$, a, b are end points of domain and N are grid points. k_1, k_2 are being taken as zero in all cases except for problem 4, where there values are mentioned. The number of stencil size are taken as $ns = 4(M(M+1)/2)$ while number of points on interface are taken 150 in all test problems. For error analysis, the L_∞ norm is employed. All the problems are solved on Laptop Dell Core 5 having 4 GB RAM.

Test Problem 1 ([17]). Let us consider the Poisson equation (1) in 2D on a domain $[-1, 1] \times [-1, 1]$ having star shape interface, having oscillations with $\kappa = 3$ inside the sub-domain, the discontinuous coefficients are taken as $\beta_2 = 3$ and $\beta_1 = 5$. The exact solution of PDE is,

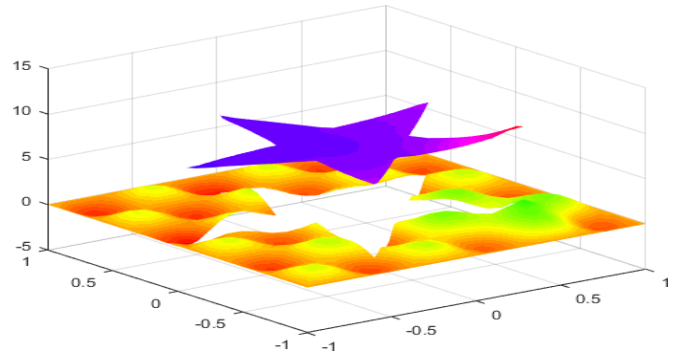

Figure 3: Graphical representation of the numerical solution for test problem 1.

$$U_1 = x^2 + y^2 + 7, if\ (x,y) \in \Omega_1,$$

$$U_2 = \sin(k\pi x)\sin(k\pi y), \qquad if\ \ (x,y) \in \Omega_2$$

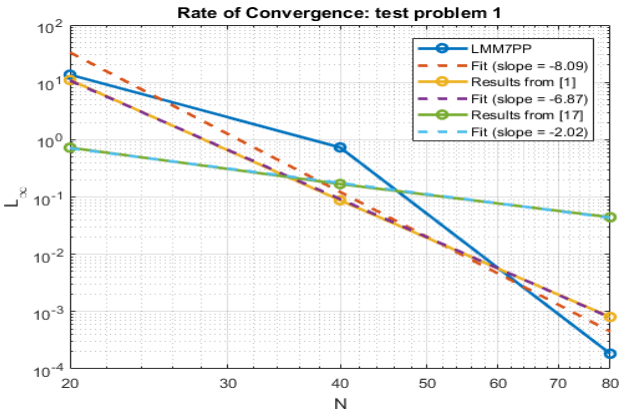

Figure 4: Rate Of Convergence Correspond To Test Problem 1.

The results correspond to problem 1 are given in fig 4 and table 1. The rate of convergence of proposed method in fig 4 is higher than [1] and [17]. As the graph go down from left to right, therefore the slope is negative. Also we compared results at each corresponding point in table 1.

N	LMM7PP	Grad	Courtesy [1]	Courtesy [17]
20	$1.36e+01$	$1.65e+02$	$1.10e+01$	$7.25e-01$
40	$7.31e-01$	$1.78e+01$	$8.74e-02$	$1.68e-01$
80	$1.84e-04$	$2.09e-02$	$8.05e-04$	$4.43e-02$

Table 1: Comparison of error of problem 1 with [17] and [1].

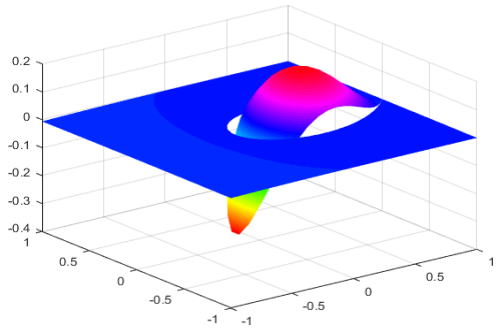

Figure 5: Graphical Representation of The Numerical Solution for Test Problem 2.

Test Problem 2 ([18]). Consider an elliptic interface problem described by equation (1), featuring a distinctive interface shaped like half of a Lemniscate. Notably, one of the interface's corners extends sharply to the outer boundary. The analytical solution for this particular problem is provided by, $U(x,y) = \frac{((x-1)\tan(\theta))^2 x - y^2)}{\beta(x,y)}$,

in which $\theta = 40$ are taken. Also $\beta_1 = 1$ and $\beta_2 = 1000$.

$N \times N$	LMM7PP	Grad	LMM9PP	Grad
20	$4.29e-15$	$2.58e-13$	$9.34e-15$	$5.05e-13$
40	$1.12e-13$	$3.86e-12$	$6.22e-15$	$1.32e-12$
80	$1.01e-13$	$2.24e-11$	$1.92e-13$	$1.47e-11$

Table 2: Error Correspond to Problem 2 Upon Interface of Star Shapes Using Uniform Nodes.

H	LMM7PP	Grad	LMM9PP	Grad
0.06	$1.45e-07$	$3.97e-06$	$9.76e-09$	$2.42e-07$
0.05	$1.75e-15$	$4.60e-14$	$1.98e-15$	$2.13e-13$
0.04	$9.85e-16$	$7.22e-14$	$3.16e-15$	$2.84e-13$
0.03	$2.07e-15$	$1.81e-13$	$3.28e-14$	$4.48e-12$

Table 3: Error Analysis Correspond to Test Problem 2 on Half Lemniscates Shapes Interface Using Scattered Nodes.

The high order accuracy correspond to test problem 2 are shown in Tables 2 and 3 for uniform and scattered nodes respectively. The Pohyharmonic spline with $\epsilon = 5$ is taken in both cases.

Test Problem 3 ([18]). The elliptic interface problem described by equation (1) features a deltoid-like interface structure. The analytical solution for this problem is provided as follows,

$$U(x,y) = \frac{(y^2+x^2)^{3/2}}{\beta(x,y)},$$

here $\beta_1 = 1$ and $\beta_2 = 1000$

$N \times N$	LMM7PP	Grad	LMM9PP	Grad
20	$2.39e-04$	$6.20e-03$	$2.39e-04$	$9.90e-03$
40	$8.42e-05$	$1.90e-02$	$3.01e-05$	$6.70e-03$
60	$1.12e-05$	$1.10e-03$	$1.14e-05$	$2.30e-03$
80	$5.19e-06$	$4.51e-04$	$5.12e-06$	$1.60e-03$

Table 4: Analysis of Error Correspond to Problem 3 on Interface as Star Shape Using Uniform Nodes

H	LMM7PP	Grad	LMM9PP	Grad
0.06	$5.48e-05$	$3.20e-03$	$4.90e-05$	$4.10e-03$
0.05	$2.27e-05$	$8.70e-04$	$2.04e-05$	$1.70e-03$
0.04	$1.23e-05$	$8.68e-04$	$1.17e-05$	$8.68e-04$
0.03	$2.11e-06$	$3.46e-04$	$2.04e-06$	$3.41e-04$

Table 5: Error Analysis Correspond to Test Problem 3 On Deltoid Shapes Interface Using Scattered Nodes.

The results correspond to test problem 3 are shown in tables 4 and 5 for uniform and scattered nodes respectively. In both cases the multiquadric RBF is used with $\epsilon = 7$. The accuracy improves significantly as the number of grid points increases, see table 4 and again the accuracy improves significantly as the nodal distance h decreases, see table 5.

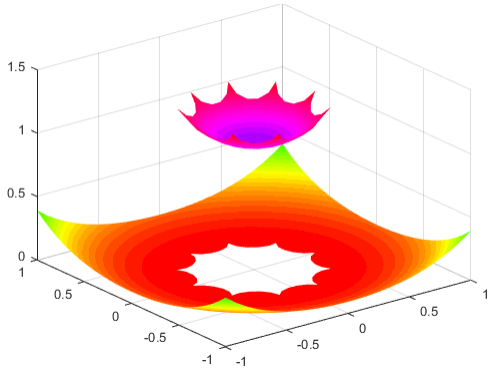

Figure 7: Graphical Representation o f The Numerical Solution for Test Problem 4.

Test Problem 4 ([19]). The elliptic interface problem defined by equation (1) features interfaces resembling both hypocycloid and epicycloid shapes. The analytical solution for this problem is provided as follows

$$U_1 = e^{x^2+y^2}, if\ (x,y) \in \Omega_1,$$

$$U_2 = -0.01 \log\left(2\sqrt{x^2+y^2}\right) + 0.1(x^2+y^2)^{3/2}, if\ (x,y) \in \Omega_2,$$

with

$$\beta_1 = 1$$

$\beta_2 = 10$ and $k_1 = k_2 = 10(x+y)$.

H	LMM7PP	Grad	LMM7PP	Grad

0.06	$2.78e-05$	$5.46e-04$	$1.62e-05$	$2.31e-04$
0.05	$7.04e-06$	$1.26e-04$	$6.84e-05$	$7.53e-04$
0.04	$1.25e-06$	$1.28e-04$	$2.16e-06$	$5.59e-05$
0.03	$2.55e-06$	$6.60e-05$	$3.48e-07$	$8.84e-06$

Table 6: Error Analysis Correspond to Test Problem 4 On Hypocycloid Shape Left and Epicycloid Shape Interfaces Right Using Scattered Nodes

The results correspond to test problem 4 on hypocycloid shape left and epicycloid shape interfaces right using scattered nodes are shown in table 6. The polyharmonic spline is used with $\epsilon = 7$. The accuracy become better as the nodal distance h decreases.

Test Problem 5 ([20]). Let us take the elliptic PDE (1) in 2D on circular shape interface with domain $[-1, 1] \times [-1, 1]$, the exact solution is given as

$$U_1 = \sin(x + y), if\ (x, y) \in \Omega_1,$$

$$U_2 = \cos(x + y), if\ (x, y) \in \Omega_2,$$

with $\beta_1 = yx, if\ (x, y) \in \Omega_1\ and\ \beta_2 = y^2 + x^2, if\ (x, y) \in \Omega_2$.

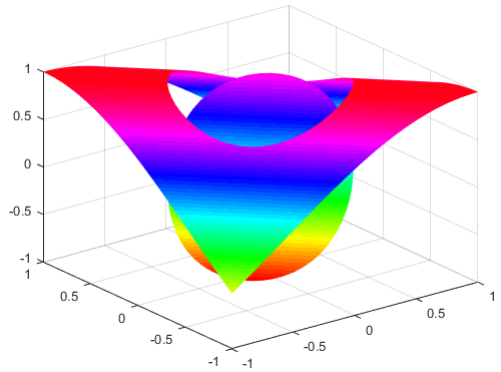

Figure 8: Graphical Representation o f The Numerical Solution for Test Problem 5.

H	LMM7PP	Grad	Number of Neurons	$e_{\Omega 1}$ [20]
0.07	$2.79e-09$	$8.60e-08$	10	$3.01e-04$
0.06	$1.87e-09$	$1.04e-07$	20	$1.93e-04$
0.05	$9.82e-10$	$7.03e-08$	40	$2.28e-04$
0.04	$5.11e-09$	$1.75e-07$		
0.03	$5.91e-11$	$1.32e-08$		

Table 7: Error Analysis Correspond to Test Problem 5 on Circular Shape Interface Using Scattered Nodes.

The results correspond to test problem 5 are shown in tab 7, in which the polyharmonic spline is used with $\epsilon = 7$. A reasonable result is achieved at each point.

4. Conclusion

In conclusion, this study introduces a local meshless method for elliptic interface PDEs, utilizing RBFs enhanced with Pascal polynomials. This approach effectively tackles complex interface geometries, showcasing both computational efficiency and accuracy.

The RBFs are combined with Pascal polynomials $\sum_{i,j=1}^{n,i} p_{ij}\, x^{i-j} y^{j-1}$ to solve the PDEs numerically. Insights from benchmark tests lead to the conclusions given below:

- The performances of the LMM7PP and LMM9PP methods are generally comparable.
- The proposed method handles weak geometrical singularities and oscillation of solution upto sufficient extent.
- The performance of the proposed method is well on both uniform and scattered data, notably achieving higher accuracy than some existing methods as discussed in literature.
- This method can be easily implemented on irregular interface geometries.

References

[1] S. Islam E. Larsson M. Ahmad. Local meshless methods for second order elliptic interface problems with sharp corners. *Journal of Computational Physics*, 416:109500, 2020.

[2] M. Zhan K. Xia and G. W. Wei. Galerkin method for elliptic interface problems. *Computa- tional and Applied Mathematics*, 272:195–220, 2014.

[3] Y. Zhou S. Yu and G. W. Wei. Matched interface and bounary (mib) method for elliptic problems with sharp-edged intefaces. *Computational Physics*, 224:729–756, 2007.

[4] R. Miniowitz and J.P. Webb. Covariant-projection quadrilateral elements for the analysis of wave-guides with sharp edges. *Trans. Microwave Theroy Technology*, 39:501–505, 1991.

[5] M. Tong G. Pan and B. Gilbert. Multiwavelet based moment method under discrete sobolev- type norm. *Microwave and Optical Technology. Letters*, 40:47–50, 2004.

[6] D. R. Tanner Z. P. Tanner, J. Z. Savage and A. F. Peterson. Two-dimensional singular vec- tor elements for finite-element analysis. *IEEE Transactions Microwave Theroy Technology*, 46:178–184, 1998.

[7] Nurtayeva Togzhan Arif S. Abdulazeez Jamal A. Salah Taha, T. Basheer. Partial differential equations and digital image processing : A review. pages 235–240, 2022.

[8] C. Cosner. A dynamic model for the ideal-free distribution as a partial differential equation.
Theoretical Population Biology, 67(2):101–108, 2005.

[9] G. Wei X. Ye L. Mu, J. Wang and S. Zhao. Weak galerkin methods for second order elliptic interface problems. *Computational Physics*, 250:106–125, 2013.

[10] D. N. Shenton Z. J. Cendes and H. Shahnasser. Magnetic field computation using delaney triangulation and complementary finite element methods. *IEEE Transactions Magnetics*, 19:2251–2254, 1983.

[11] I. Babuska and S. A. Sauter. Is the pollution effect of the fem avoidable for the helmholtz equation considering high wave number? *SIAM Jounrnal of Numerical Analysis*, 34:2392– 2423, 1997.

[12] S. Hou and X.D. Liu. A numerical method for solving variable coefficient elliptic equation with interfaces. *Computational Physics*, 202:411–445, 2005.

[13] Q. Shen. Local rbf based differential quadrature collocation method for the boundary layer problems. *Engineering Analysis with Boundary Elements*, 34:213–228, 2010.

[14] R. Schaback. Error estimates and condition numbers for radial basis function interpolation.
Advances in Computational Mathematics, 3:252–264, 1995.

[15] S. A. Sarra. Integrated multiquadric radial basis function approximation methods. *Comput- ers and Mathematics with Applications*, 51(8):1283–1296, 2006.

[16] B. Fornberg and G. Wright. Stable computation of multiquadric interpolants for all values of the shape parameter. *Computer and Mathematics with Applications*, 48(5-6):853–867, 2004.

[17] M. Zhanb K. Xiaa and G. W. Wei. Mib galerkin method for elliptic interface problems.
Journal of Computational and Applied Mathematics, 272:195–220, 2014.

[18] H. Guo and X. Yang. Gradient revovery for elliptic interface problem: II. Immersed finite element methods. *Journal of Computational Physics*, 338:606–619, 2017.

[19] S. Islam and M. Ahmad. Meshless analysis of elliptic interface boundary value problems.
Engineering Analysis with Boundary Elements, 92:38–49, 2017.

[20] F. Gao F. Cao, X. Guo and D. Yuan. Deep learning nonhomogeneous elliptic interface problems by soft constraint physics-informed neural networks. *Mathematics*.